ENHANCING FILM COOLING EFFECTIVENESS IN A GAS TURBINE END-WALL WITH A PASSIVE SEMI CYLINDRICAL TRENCH

by

Duraisamy RAVI [*] ***and Kanjikovil Mahali PARAMMASIVAM***

Department of Aerospace Engineering, MIT Campus, Anna University, Chennai, India

Original scientific paper
https://doi.org/10.2298/TSCI170412001R

Computational studies were carried out in the end-wall of a linear cascade, of chosen blade profile, which is provided with one row of cylindrical film cooling holes inclined at 30° to the end wall. The CO_2 gas was used as the coolant supplied through the film holes, maintaining a blowing ratio of 0.6. The film cooling hole row was positioned at the leading edge of the cascade. The mainstream fluid was air and based on its properties at the cascade inlet, the flow was found turbulent. A semi cylindrical trench was placed at two positions upstream of the cascade leading edge and three positions downstream of it. ANSYS FLUENT 15.0 was used to compute the film cooling effectiveness of the cascade endwall. Trench positioned at a distance of twice that of film hole diameter, was found to show a highest increase of area averaged effectiveness value by 30.4% over the baseline. Further to this, the influence of the trench diameter was carried out where the trench with diameter twice that of film hole diameter was found to show a 31.3% increase of cooling effectiveness over the baseline. Studies on the influence of blowing ratio showed a highest increment of cooling effectiveness value by 43.5% over the baseline a blowing ratio of 1.2.

Key words: *end wall film cooling, passive device cooling, CFD analysis, adiabatic effectiveness.*

Introduction

The predominant mode of cooling in the case of a gas turbine cascade end wall is film cooling. In the film cooling technique, a relatively cold fluid with respect to the hot combustion gases is released from discrete holes. This cold fluid forms a thin film layer on the surfaces to be protected and hence called film cooling. Film cooling technique is being employed in gas turbines as a life enhancing method for both the turbine blades and end walls, which are directly in contact with the high temperature gas from the turbine combustion chamber. The surface is protected by the avoidance of the hot combustion gases to contact the surface directly. Film cooling technique works through the principle of convective cooling, where adiabatic cooling effectiveness, η, was used to assess the film cooling performance.

The configuration of the film cooling geometry is important as it decides the film cooling coverage on the surface under study. Film cooling is being employed on the first stage blades of gas turbines, both stationary and rotating. A large volume of literature on film cooling is available in this domain and considerable research work can be found in the context of end wall cooling and its enhancement. Ligrani and Lee [1] have discussed the fluid dynamic behaviour of one row compound angled film cooling holes (FCH) at different blowing ratios, *M*. A similar flow field study was reported by Tyagi and Acharya [2], whereas Gritsch *et al.* [3] measured the coefficients of discharge for several configurations of cylindrical film holes.

Corresponding author, e-mail: ravivsravi.aero@gmail.com

Flow characteristics, film cooling effectiveness, and heat transfer coefficient distribution are studied by Xie *et al*. [4]. Effect of turbulence intensity at the inlet, curvature of the surface and the shape of the hole on η was reviewed by Bogard and Thole [5]. Reynolds stress model (RSM) turbulence model was used by Nemdili *et al.* [6] for leading edge film cooling of a symmetrical turbine blade model. They found the yield from the second order RSM has reasonably good agreement with measurement data. Baheri *et al.* [7] have presented investigations on a row of film cooling holes in a flat plate with simple and compound inclinations. A correlation between the parameters η, M, hole coverage ratio, area ratio, and hole spacing was studied by Colban *et al.* [8] using the data from literature. Li and Hassan [9] proposed that the intensity of the counter rotating vortex pair, as an alternate parameter to the blowing ratio, that defines η. The convective heat transfer coefficients along the surface of the objects placed inside the system are determined by Kewou and Edoun *et al.* [10] and the performance of flow and heat transfer is analyzed in a microturbine system. by Gui and Song [11].

Apart from these studies with regular or novel film hole geometries, several researchers have worked on the passive flow control devices that could enhance the heat transfer performance. Improvement in turbine endwall flow uniformity by controlling secondary flows was studied by Thomas and Povey [12]. Micha Prem Kumar [13] has investigated the numerical method for temperature distribution in turbine vane cooling with rib and parabolic turbulator with reference to the smooth channel has been presented. Lu *et al.* [14] have built a transient infrared thermography set-up and tested a non-trenched and four trenched configurations accomplished with inserts. Waye and Bogard [15] have conducted high resolution measurements of η of simple axial FCH embedded in a transverse trench with various trench configurations.

It can be observed that, several studies on one or multiple row FCH, with simple or compound angles of inclination, with different holes shapes were performed and reported in open literature. Apart from active film holes, passive flow control devices such as film holes in rectangular trenches or contoured craters were also tested for end-wall effectiveness improvement. However, the influence of a passive device such as a semi-cylindrical trench (SCT), covering the full transverse pitch of the cascade, was not studied and reported so far. Hence the objective of the present study is to conduct numerical computations of a SCT placed on the end-wall of a linear gas turbine cascade, which is cooled by a single row of film holes positioned at the leading edge line. The influence of SCT was studied by positioning it at strategic locations, upstream or downstream of the FCH row. The flow and heat transfer characteristics of the system under study is reported.

Physical domain

A linear gas turbine cascade was fabricated and tested using the profile of Gratton [16]. Computations using CFD was also carried out. The photograph of the experimental set-up fabricated for estimating the adiabatic end-wall film cooling effectiveness is shown in fig. 1. Compressed air was supplied from a bank of compressors and was made to pass through a settling chamber where the flow velocity got reduced. From the settling chamber, the air flow velocity is increased again, when it entered the constant cross-sectional rectangular test section. The test section was constructed with acrylic sight windows fixed on a mild steel base. From the Taguchi coupled CFD analysis [17], the optimal location of the film cooling row was found to be at the leading edge of the cascade *i.e.*, $x/d_f = 0$, and is used presently.

Computational domain

Taking advantage of the periodic nature of the cascade, in the pitch-wise transverse direction, the flow passage between two adjacent blades was considered as the computational

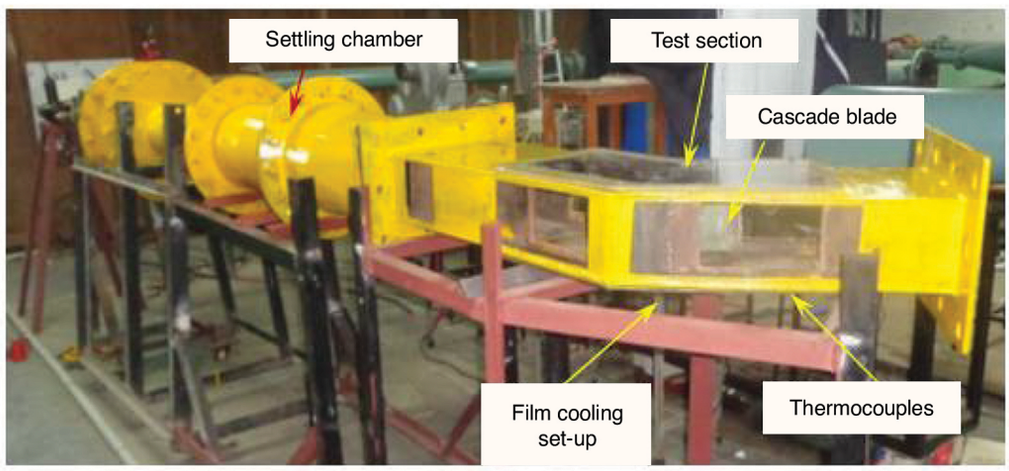

Figure 1. Experimental gas turbine cascade set-up [17]

domain as shown in fig 2(a). The domain was split within the pre-processor strategically, to generate a finite volume mesh with hexahedral elements. The single row of simple FCH of diameter, d_f, making an inclination $\alpha = 30^{\circ}$ to the mainstream was considered. Figure 2(b) shows the FCH row located at the leading edge of the gas turbine cascade *i.e.*, $x/d_f = 0$. The SCT covering the full transverse pitch (= 22 d_f) of the cascade, between the PS and SS of the cascade, positioned at $x/d_f = -2$ is also shown. For a chosen pitch of $2d_f$, 12 film holes, whose dimensions are shown in fig. 2(c), can be accommodated on the end-wall. From the Taguchi coupled CFD analysis [17], the optimal location of the film cooling row was found to be at the leading edge of the cascade *i.e.*, $x/d_f = 0$, and is used presently. The geometrical and flow parameters of the gas turbine cascade tested presently are summarized in tab. 1.

Numerical methodology

Grid independency

Hexahedral meshing was done for the computational domain with strategic splitting of the domain. Discretization of the domain was done with three different mesh size settings to produce meshes with 2.7, 4.8 and 9.8 million cells, to study the grid independency for the cascade with FCH positioned at $x/d_f = -8$.

The averaged adiabatic effectiveness, estimated over the end-wall region shown in the inset figure between $x/d_f = -8$ and $x/d_f = +20$, was plotted against the mesh density as shown in fig. 3. The variation of the η value between 4.8 million cells and 9.8 million cells was 2.2% only and hence 4.8 million cell density is adequate for this study and used.

Table 1. Geometrical parameters of the gas turbine cascade tested presently

Parameter of the blade	Unit	Value
Blade actual Chord, C_h	mm	107.3
Blade pitch to chord ratio, P/C_h	–	0.9086
Blade height to chord ratio, H/C_h	–	1.34
Reynolds number,	–	2e+5
Mainstream fluid, *m*	–	Air
Coolant fluid, *c*	–	Co_2
Coolant to mainstream density ratio, P_c/P_m	–	1.46
Prandtl number of mainstream, coolant fluid	–	0.71, 4.1
Blowing ratio, *M*	–	0.6, 0.8, 1.0, 1.2
Film hole diameter, d_f	mm	4
Film hole pitch to hole diameter ratio, P_f/d_f	–	2.0
Film hole length to hole diameter ratio, l_f/d_f	–	3

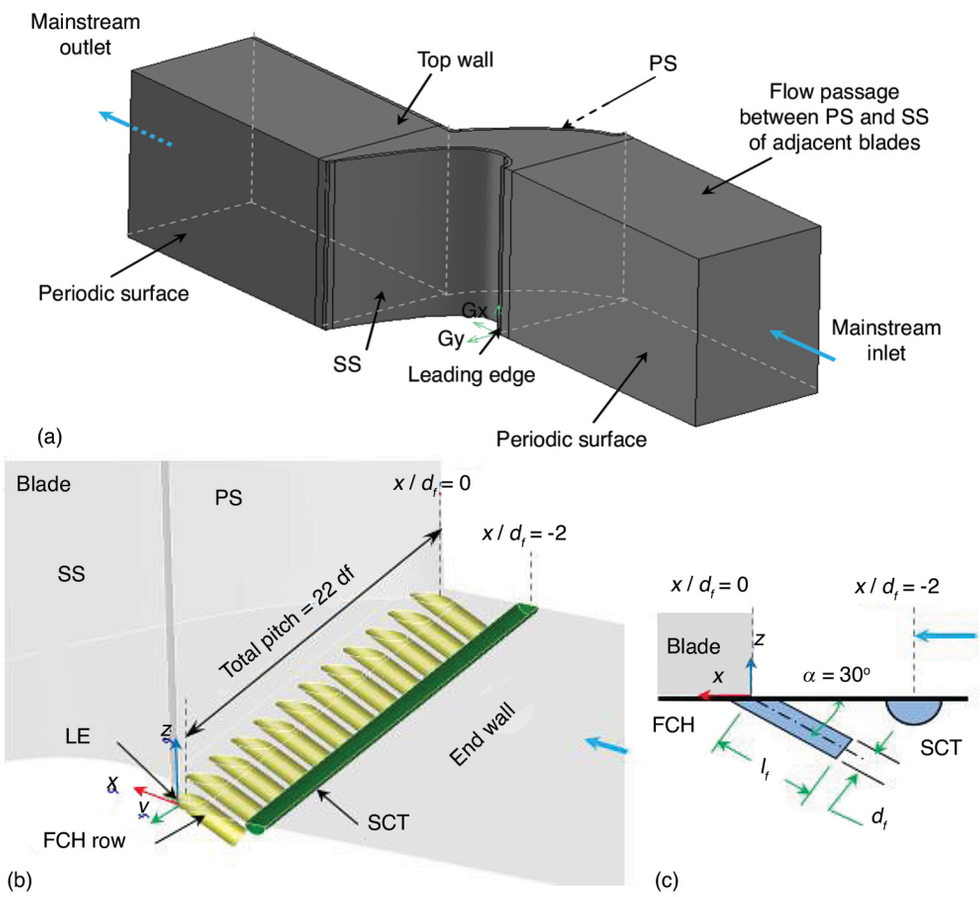

Figure 2 Geometry details of the cascade presently studied; (a) cascade mainstream flow domain (without FCH, SCT) [17], (b) location of SCT with reference to LE, and (c) details of the FCH, SCT

Solver details

The 3-D, steady-state, incompressible turbulent flow simulations were carried out with different configurations of single passage domain of the film cooled gas turbine cascade. Details of the governing equations and the numerical formulation employed can be found from ANSYS FLUENT documentation [18]. The SIMPLE algorithm, details of which can be found in Patankar [19], was chosen for coupling the pressure and velocity terms. Further to Vickery and Iacovides [20], Realizeable k-ε model with enhanced wall treatment option in the solver Fluent was chosen for the present computations. The mainstream inlet was specified with a constant velocity of 30 m/s at a temperature of 303 K for all the cases. The convergence criteria for the computational solution were determined based on scaled residuals for the equations of continuity, momentum equations and turbulence quantities. The scaled residuals for solution convergence were set to 10e-5 for all governing equations and turbulence quantities.

The ANSYS FLUENT 15.0 was used for the numerical computations with air as the hot gas and CO_2 gas as the coolant. Interfaces were created in the solver, between FCH, SCT and the cascade end-wall. This *interface* option in the solver helps in positioning the FCH and SCT along the stream-wise direction without any need to modify the cascade mesh for each change in

position. The mesh in the mainstream cascade domain is the same for all cases studied presently, thus ensuring consistency and accuracy in the results. The bottom wall in the experiments was insulated. In-line with this, the external wall in the numerical simulations can be modelled as *adiabatic* and hence the wall thickness need not be modelled in the numerical simulations, as the plate will attain uniform temperature without any thermal loss to ambient.

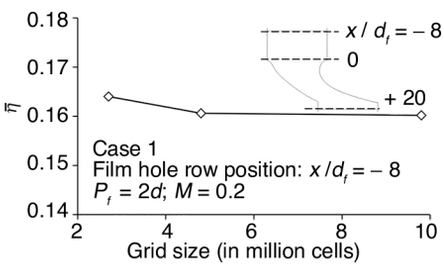

Figure 3. End-wall averaged $\bar{\eta}$ variation with different grid sizes

Data reduction

The blowing ratio, M, is the ratio of the mass flux of the coolant fluid to that of the mainstream fluid, and is defined:

$$M = \rho_c V_c / \rho_m V_m \tag{1}$$

where ρ_c, V_c, and ρ_m, V_m are density and velocity of the coolant and mainstream respectively.

Reynolds number at the mainstream inlet based on the properties of the mainstream fluid at the inlet was estimated using:

$$\mathrm{Re} = \rho_m V_m C_h / \mu_m \tag{2}$$

where μ_m is the viscosity of mainstream at the cascade inlet and C_h is the blade actual chord length.

The FCH effectiveness, η, is calculated using the following equation:

$$\eta = (T_{m,\mathrm{in}} - T_w) / (T_{m,\mathrm{in}} - T_{c,\mathrm{in}}) \tag{3}$$

where $T_{m,\mathrm{in}}$, T_w and $T_{c,\mathrm{in}}$ are the temperatures of mainstream at inlet, wall and coolant at the inlet. The pitch-wise length averaged, η, is the average of the local values along the chosen line and is denoted as η_p whereas the end wall area averaged value is identified as $\bar{\eta}$.

Results and discussions

Influence of SCT position

Figure 4 shows the distribution of η on the turbine cascade end-wall for chosen SCT positions, with the diameter of the SCT same as that of the FCH *i.e.*, $d_t = d_f$ for a blowing ratio $M = 0.6$. The pattern variation in the coolant flow can be observed from the contours.

The distribution pattern of η for the FCH only case, without SCT is shown in fig. 4(a). The cross-flow of the mainstream fluid adjacent to the end-wall, from PS side to the SS side can be observed as shown with arrowheads in fig. 4(a). This cross-flow is caused by the induced secondary flow close to the end-wall. This kind of cross flow is produced as a result of the gradient in pressure between PS and SS surfaces. The adiabatic effectiveness value increases with the positional change of the coolant row location oriented towards the downstream side. Higher spreading of the coolant was found when the FCH was positioned at $x/d_f = 0$.

Region 'A' highlighted in fig. 4(a) identifies the region closer to the end-wall – PS intersection, where the fluid starts moving from the PS to the SS and the value of η decreases further downstream from this point. Region 'B' highlights the zones of low η on the end wall, immediately downstream of adjacent film holes.

Figures 4(b)-(f) show the distribution of for SCT positioned at $x/d_f = -4, -2, +2, +4$, and +6, respectively. Figure 4(b) shows the region 'B' got as a clearly identifiable low η region. But the spread of improved values of η was found to be increased near region 'A'. This improvement was found to be the best for SCT positioned at $x/d_f = -2$, as in fig. 4(c). When the SCT was moved further downstream to $x/d_f = +2$, as in fig. 4(d), the low regions in the region 'B' got

improved and the distribution pattern was found better. Moving the SCT further downstream did not help in improving the distribution pattern, as observed in figs. 4(d) and 4(e).

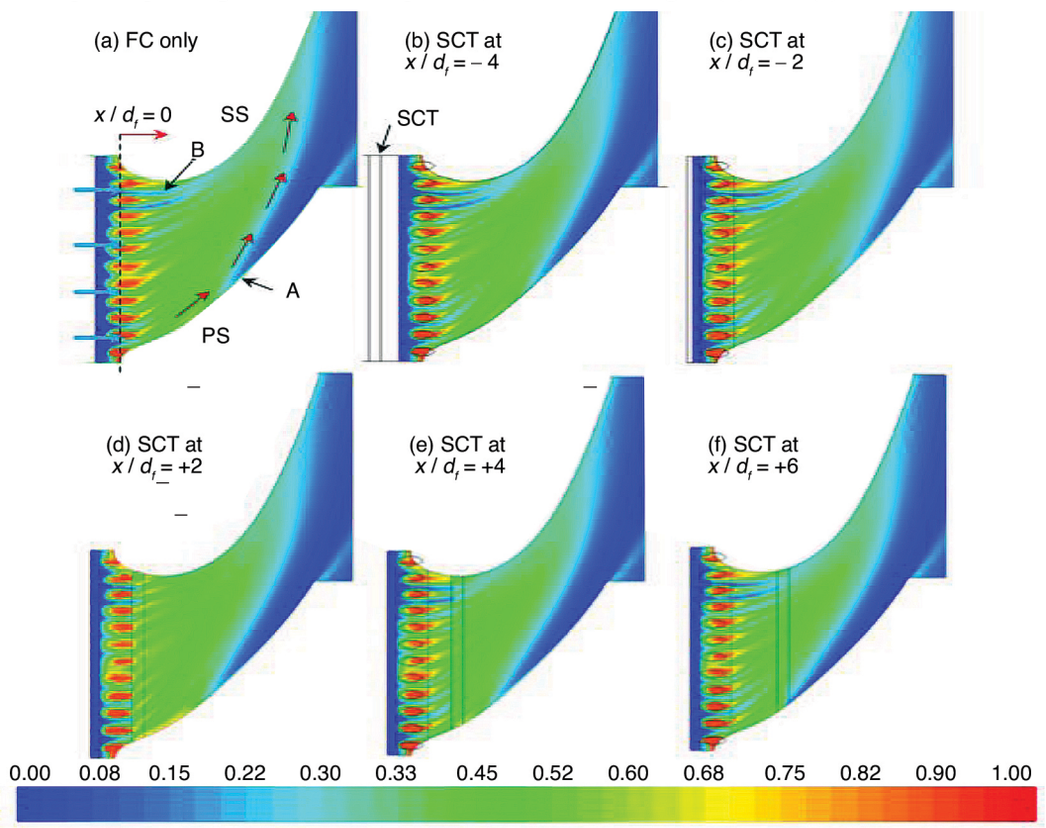

Figure 4. Contours of η on the end-wall with SCT at different locations (M = 0.6, FCH at x/d_f = 0)

Figure 5 shows the variation of end-wall area averaged effectiveness value, η, with the location of the SCT on the end-wall at a blowing ratio M = 0.6 and FCH positioned at x/d_f = 0. The η value for the FCH only case (x/d_f = 0) was estimated to be 0.33. Adding a SCT was found to enhance the end-wall effectivness more than in the baseline case. This indicates that a passive device such as a SCT could help to improve the turbine cascade end-wall effectiveness. The positioning of the SCT was estimated at x/d_f = −2 showed a highest increment in end-wall area averaged effectiveness, η, up to 30.4% when compared to the end-wall with FCH only, without SCT.

A detailed performance analysis was carried out along several chosen lines on the end-wall, in the pitch-wise direction. The variations of η_p in the stream-wise direction, along chosen lines, is shown in fig. 6 for SCT with diameter $d_t = 1.0\ d_f$ and FCH at x/d_f = 0, at different SCT positions (x/d_f locations). When the SCT was positioned immediate downstream of the FCH row, highest values of η_p reaching up to 0.75. The values of η_p are found to decrease when the SCT was positioned further downstream and the shifting trend of the peak values show the secondary flow movement from the PS to the SS as discussed earlier. The SCT positioned at x/d_f = +2 showed high values of η_p between x/d_f = 2 and 8. The SCT positioned at x/d_f = –2 can be seen showing the highest value of η_p for a wider stream-wise length from x/d_f = 8 to 20.

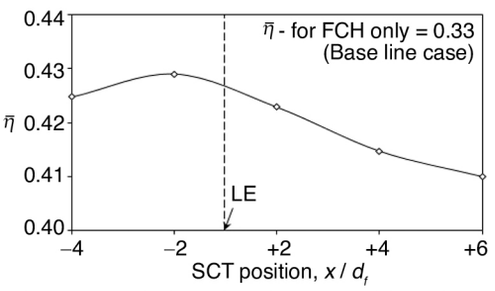

Figure 5. Variation of $\bar{\eta}$ with the position of SCT (M = 0.6, FCH at x / d_f = 0)

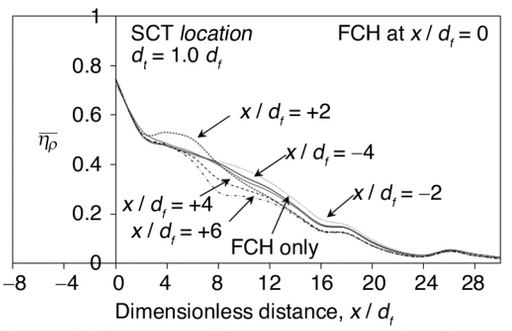

Figure 6. Variation of $\bar{\eta}_p$ in the stream-wise direction at different SCT positions

Figure 7 shows the stream traces of the fluid-flow on the end-wall as viewed from the cascade top. Figure 7(a) shows the traces on the end-wall for the baseline case *i.e.*, simple uncooled mainstream flow in the cascade without any FCH or SCT. The development of horse-shoe vortex (location 'A'), merging of PS and SS legs (location 'B') of the horse-shoe vortex and its development into the passage vortex (location 'C'), can be observed. When FCH was introduced in the cascade to protect the end-wall, the flow dynamics adjacent to the end-wall changed drastically as observed in fig. 7(b). The horse shoe vortex pattern got affected due the introduction of the FCH and the imprint of the FCH row can also be seen in the same figure. The passage vortex was found to collapse and the coolant flow was found to flow in segregated passages. However the secondary flow movement due to the geometric curvature and pressure gradient pushed the coolant flow from the PS towards the SS.

Figure 7(c) shows the stream traces on the end-wall of the cascade with FCH and SCT. The trench diameter d_t = 1.0 d_f and located at x/d_f =−4. The modified flow pattern adjacent to the end-wall due to the addition of the SCT can be observed in fig. 7(c). Due to the presence of the passive device SCT upstream of the FCH, the flow gets a more guidance downstream. This helps in improving the film cooling effectiveness η on the end-wall and η was estimated at 29.1% higher than the corresponding value in the baseline case.

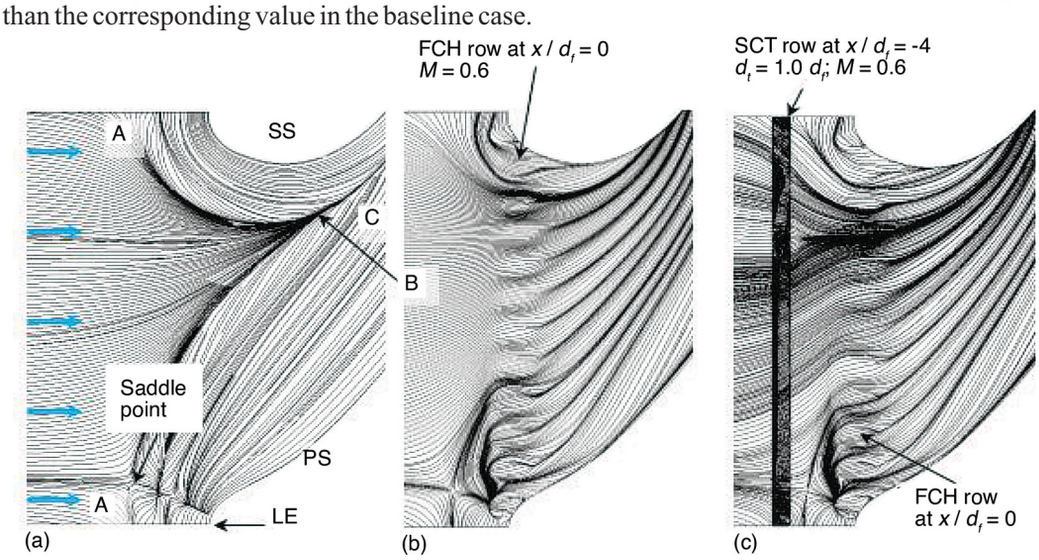

Figure 7. Traces of the fluid-flow on the end-wall; (a) Baseline - no FCH, SCT, (b) FCH only, (c) FCH and SCH

Figure 8 shows the stream traces on the SCT surface for enabling understanding of the local dynamics of the mainstream fluid. The fluid adjacent to the end-wall was found to fall into the SCT. This can be identified by a separating line (marked 'D') formed due to the re-circulation of mainstream fluid within the SCT. When the fluid was coming close to the LE, due to the horse shoe vortex formation, the fluid was made to squeeze in the spacē available. This can be inferred from fig. 8(a) where a dark separating line can be found moving closer to each other, from the region marked 'A' on the PS and SS. This flow convergence in the mainstream fluid upstream of the LE, creates an interaction as seen from region marked 'E', refer fig 8(b). This falling of fluid adjacent to the end-wall into a passive device like SCT also can be expected to keep the main-stream fluid closer to the end-wall, thus enhancing better mixing of hot and cold fluids.

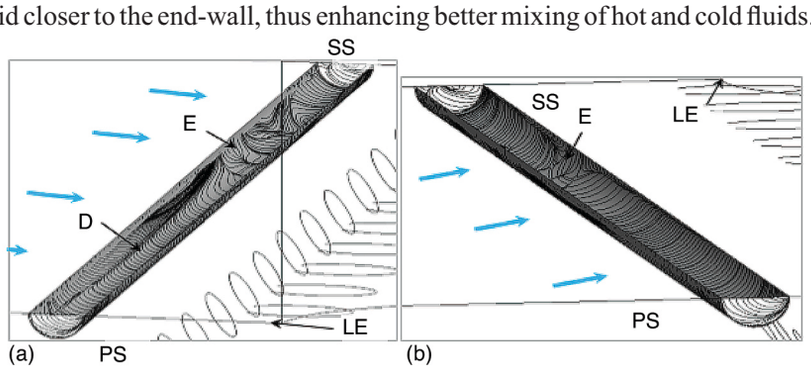

Figure 8. Traces of the fluid-flow on the SCT surface (a) view from LE side, (b) view from channel inlet side

Influence of SCT diameter

Further to the computations on the influence of SCT position, the numerical studies were extended to study the influence of SCT diameter. From the SCT position study, it was found that the SCT positioned at $x/d_f = -2$ gave the best enhancement in η Since the location $x/d_f = -2$ cannot accommodate further increase in SCT diameter, as it interfered with the inclined film hole geometry, the influence of SCT diameter study was carried out with the SCT positioned at $x/d_f = -4$.

Figure 9 shows the distribution of η on the cascade end-wall with different SCT diameters, with the SCT positioned at $x/d_f = -4$. The increased η distribution on the end-wall with

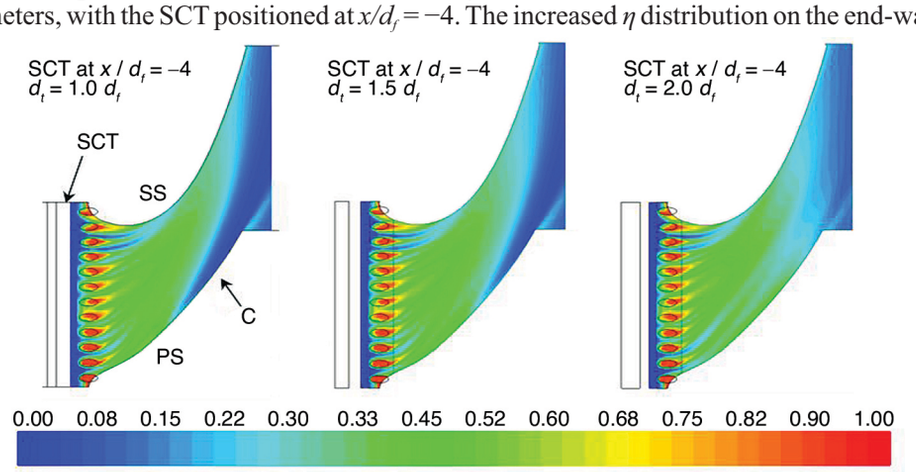

Figure 9. Contours of η on the end-wall with different SCT diameter (d_t)

increased d_t can be clearly understood from the distribution contours. Region C highlighted in the figure which showed lower η values for $d_t = 1.0d_f$, was found to show higher values with $d_t = 2.0d_f$. The value of η for the $d_t = 1.5d_f$ was found to be 30% and the highest increment in η of 31.2% was observed for $d_t = 2.0d_f$.

Influence of blowing ratio

The impact of M on the end-wall was carried out with SCT at the best location ($x/d_f = -4$) with the best diameter ($d_t = 2d_f$) identified earlier. The η distribution on the end-wall for different values of blowing ratio is plotted in fig. 10. It can be observed that η increases with M. A highest increment in $\overline{\eta} = 43.5\%$ was found for $M = 1.2$.

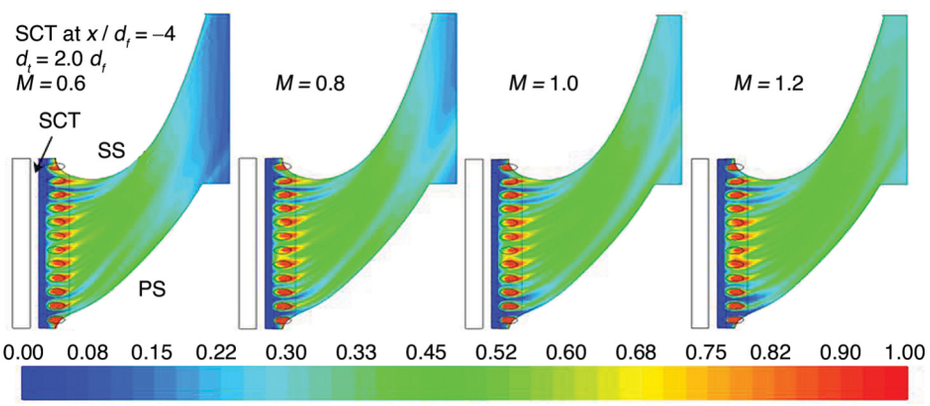

Figure 10. Contours of η on the end-wall with different blowing ratio M

Validation method

The computational results need to be validated against the present experimental results, to gain confidence in the present computation approach. The computation were carried out for a combination of FCH row position, blowing ratio which were similar to the experiments. The FCH row was positioned at the stream-wise location $x/d_f = -8$ and the blowing ratio was maintained at $M = 0.2$. The experimental static pressure values and the temperature values in terms of adiabatic film cooling effectiveness, η, were compared with those of the computational measurement on the same locations of the end-wall. For baseline configuration we have chosen the blowing ratio 0.2 which is sufficiently enough to validate the existing computational results of the tested conditions. Where as in the passive device the flow conditions,we have tested the blowing rato of upto 1.2 which is well agreeable within the limits for the tested condition.

Uncertainty estimate

Uncertainty analysis is needed to prove the accuracy of the experimental measurements. In this study, uncertainty analysis focuses on the measured and calculated parameters. An assessment of the deviation of the measured value from the actual value is important and it is estimated here.

The uncertainty estimates in the adiabatic film cooling effectiveness, [η], following eq. 3, can be found as a function of three temperatures $T_{m,\text{in}}$, T_w, and $T_{c,\text{in}}$. The estimated uncertainty [ω_η] in can be written:

$$\omega_\eta = \left[\left(\frac{\partial\eta}{\partial T_{m,\text{in}}}\omega_{Tm,\text{in}}\right)^2 + \left(\frac{\partial\eta}{\partial T_w}\omega_{Tw}\right)^2 + \left(\frac{\partial\eta}{\partial T_{c,\text{in}}}\omega_{c,\text{in}}\right)^2\right]^{1/2} \tag{4}$$

To estimate the experimental uncertainties in the results presented, the approach described by Holman [21] was applied. Based on these the maximum uncertainty in η was estimated to be 4.5%.

Conclusions

Numerical studies were carried out on a linear gas turbine cascade, with one row of FCH and compounded with a trench. The studies were reported with the FCH row positioned at stream-wise location $x / d_f = 0$ *i.e.*, at the leading edge. The CFD analyses were carried out with Realizable k-ε model for turbulence closure. Highest values of averaged η were observed in the proximity of FCH, with the peak value of $\bar{\eta}_p$ near the coolant comes out of the holes and found to decrease further downstream. The flow pattern study revealed the characteristics of the hot and cold fluids in the cascade. The fluid dynamic behaviour of the mainstream and the coolant mixture in the cascade flow passage with FCH and SCT is presented.

Numerical studies carried out on the cascade with SCT at various chosen positions revealed that when the SCT was placed at $x / d_f = -2$, the end-wall showed the highest increment in the η up to 30.4% compared to that with FCH only case. Computational investigations to study the influence of d_t showed that a highest increment in the $\bar{\eta}$ value of 31.3% was observed with $d_t = 2\ d_f$. The SCT with $d_t = 2d_f$ positioned at the best x/d_f location was used to study the influence of blowing ratio, by varying $M = 0.8$, 1.0, and 1.2. The results showed that $M = 1.2$ showed the best increment of 43.5% increase of η over the baseline.

Nomenclature

C_h – actual chord of the blade profile, [m]
d_f – film hole diameter, [m]
H – blade height, [m]
l – film hole length, [m]
d_t – trunch diameter, [m]
M – blowing ratio, ($= \rho_c \cdot V_c / \rho_m \cdot V_m$), [–]
P – blade pitch in the cascade, [m], film hole pitch, [m], pressure, [Pa] from LE to TE, [m]
Re – reynolds number ($= \rho_m V_m C_h / \mu_m$), [–]
T – temperature of fluid / wall, [K]

Greek symbols

α – film hole inclination angle, [°]
ρ – density, [kgm^{-3}]
η – adiabatic film cooling effectiveness, [–]
ω_η – uncertainty, [–]

Subscripts

c – coolant
f – film
m – mainstream
p – pitch wise
w – wall

Superscripts

- – averaged property being discussed

Acronyms

FCH – film cooling hole
LE – leading edge of the blade
PS – pressure side of the blade
SCT – semi cylindrical trench
SS – suction side of the blade

References

[1] Ligrani, P. F. M., Lee, J. S., Film Cooling from a Single Row of Compound Angle Holes at High Blowing Ratios, *International Journal of Rotating Machinery*, *2* (1996), 4, pp. 259-267
[2] Tyagi, M., Acharya, S., Large Eddy Simulation of Film Cooling Flow From an Inclined Cylindrical Jet, *ASME Journal of Turbomachinery*, *125* (2003), 4, pp. 734-742
[3] Gritsch, M., *et al*., Effect of Cross Flows on the Discharge Coefficient of Film Cooling Holes with Varying Angles of Inclination and Orientation, *ASME Journal of Turbomachinery*, *123* (2001), 4, pp. 781-787
[4] Xue, Y.-H., *et al.*, Numerical Study On Film Cooling And Convective Heat Transfer Characteristics In The Cutback Region Of Turbine Blade Trailing Edge *Thermal Science*, *20* (2016), Suppl. 3, pp. S643-S649
[5] Bogard, D. G.,Thole, K. A., Gas Turbine Film Cooling, *AIAA Journal of Propulsion and Power*, *22* (2006), 2, pp. 249-270
[6] Nemdili, F., *et al*., Reynolds Stress Transport Modeling of Film Cooling at the Leading Edge of a Symmetrical Turbine Blade Model, *Heat Transfer Engineering*, *29* (2008), 11, pp. 950-960

[7] Baheri, S. *et al*., Film Cooling Effectiveness from Trenched Shaped and Compound Holes, *Heat and Mass Transfer*, *44* (2008), 8, pp. 989-998
[8] Colban, W. F., *et al*., A Film-Cooling Correlation for Shaped Holes on a Flat-Plate Surface, *ASME Journal of Turbomachinery*, *133* (2011), 1, pp. 01002-1- 11
[9] Li, H. M., Hassan, I., The Effects of Counter Rotating Vortex Pair Intensity on Film-Cooling Effectiveness, *Heat Transfer Engineering*, *36* (2015), 16, pp. 1360-1370
[10] Kewou, S., Edoun, M. Numerical Simulation of Convective Heat Transfer Coefficient in Channel With Corrugated Walls, *Thermal Science*, *22* (2018), 1, pp. 87-100
[11] Gui, X., Song, X., Analysis on Three-Dimensional Flow and Heat Transfer in a Cross Wavy Primary Surface Recuperator for A MicroTurbine System, *Thermal Science*, *19* (2015), 2, pp. 489-496
[12] Thomas, M., Povey, T., Improving Turbine Endwall Cooling Uniformity by Controlling Near-Wall Secondary Flows, *Proceedings of the Institution of Mechanical Engineers, Part G: Journal of Aerospace Engineering*, *231* (2016), 14, pp. 2689-2705
[13] Micha Prem, Kumar, T., *et al.*, Conjugated Heat Transfer Analysis of Gas Turbine Vanes Using MacCorMack's Technique, *Thermal Science*, *12* (2008), 3, pp. 65-73
[14] Lu, Y., *et al*., Film Cooling From a Row of Holes Embedded in Transverse Trenches, 2005, *Proceedings,* ASME Paper No. GT2005-68598, ASME Turbo Expo 2005, Reno, Nev., USA
[15] Waye, S. K., Bogard, D. G., High-Resolution Film Cooling Effectiveness Measurements of Axial Holes Embedded in a Transverse Trench With Various Trench Configurations, *ASME Journal of Turbomachinery*, *129* (2007), 2, pp. 294-302
[16] Gratton, A. R., Measurements and Predictions of Heat Transfer for a First Vane Design, M. Sc. thesis, Virginia Polytechnic Institute and State University, Blacksburg, Va, USA, 2004
[17] Ravi, D., Parammasivam, K. M., Taguchi Based Regression Analysis of End-Wall Film Cooling in a Gas Turbine Cascade with Single Row of Holes, *International Journal of Turbo & Jet Engines, 33* (2015), 3, pp. 275-292
[18] ***, Ansys Fluent 15.0 User Manual Documentation (2013) SAS IP, Inc.
[19] Patankar, S.V., *Numerical Heat Transfer and Fluid Flow*, Hemisphere, Washington, D.C., 1980
[20] Vickery, W., Iacovides, H., Computation of Gas Turbine Blade film cooling, *Proceedings*, 11th UK National Heat Transfer Conference, London, 2009
[21] Holman, J. P., *Experimental Methods for Engineers*, 7th ed., Tata McGraw-Hill Publishing Company Limited, New Delhi

Paper submitted: April 12, 2017
Paper revised: September 13, 2017
Paper accepted: December 28, 2017